Assessment of Rapid Urbanization Effects with Remote Sensing Techniques

Nur Yagmur, Adalet Dervisoglu, and B. Baha Bilgilioglu

Abstract Istanbul is the most populous city in Turkey. The population, which was approximately 5.5 million in 1985, has reached 15.5 million in 2020. Population growth is the most important factor behind human activities that put pressure on the environment. An increasing population means depletion of limited resources, increasing environmental problems, and rapid urbanization. In parallel with the increase in population and urbanization, there has also been an increase in demand for housing, leading to new residential areas in almost every district of Istanbul. This study examined the transformation from vegetation areas to residential areas between 1985 and 2020 in a selected region in Buyukcekmece, one of the 39 districts of Istanbul. The relationship between land use and land cover (LULC) change in the area and Land Surface Temperature (LST) change caused by urbanization was analyzed. It is seen that the built-up area has increased from 57.1 ha to 781.4 ha in 35 years. In every five years, an increase in surface temperatures was determined in parallel with increasing urbanization, and this increase was determined as about 5.4°C from 1985 to 2020. Also, when the temperature data of the Buyukcekmece Meteorological station is analyzed, it is seen that there has been an increase of approximately 2 ºC in air temperatures in the last five years. In addition, movements were observed in the stability of structures in rapid urbanization areas after analyzing with the PSI time series InSAR method. The main causes were determined as construction sites around the buildings and geological conditions of the ground, which are triggered by urbanization.

Keywords Rapid urbanization · NDVI · LST · PSI · Istanbul

N. Yagmur (✉) · A. Dervisoglu · B. B. Bilgilioglu
Civil Engineering Faculty, Geomatics Engineering Department, Istanbul Technical University, 34469 Istanbul, Turkey
e-mail: nyagmur@gtu.edu.tr

N. Yagmur
Engineering Faculty, Geomatics Engineering Department, Gebze Technical University, 41400 Kocaeli, Turkey

B. B. Bilgilioglu
Faculty of Engineering and Natural Sciences, Geomatics Engineering Department, Gumushane University, 29000 Gumushane, Turkey

M. Ben Ahmed et al. (eds.), *Innovations in Smart Cities Applications Volume 5*,
Lecture Notes in Networks and Systems 393, https://doi.org/10.1007/978-3-030-94191-8_46

1 Introduction

Environment and natural resources are the most basic requirements for the continuation of life on Earth and are adversely affected as consumption needs increase and demands change due to the increasing population. The world has been changing very rapidly in recent years due to human activities. One of these activities is rapid urbanization, which destroys natural resources such as water bodies [1], green spaces [2], air quality conditions [3] and changes the weather conditions (e.g., an increase in air temperature, decreased precipitation) [4]. Especially with the increase in the popularity of megacities, these cities receive immigration, and the need for shelter arises due to the increasing population. The need for shelter causes rapid urbanization, land use and land cover (LULC) are changing, natural surfaces are turning into impermeable surfaces with high thermal capacity. Remote Sensing is an effective tool with the capacity for large-scale area observation to monitor urban area expansion and the stability of structures in these urbanization sites in addition to observing natural changes on Earth. With high-frequency data acquisition and large-scale monitoring, changes on the Earth's surfaces can be monitored and be detected via active and passive satellite sensors.

The Landsat mission provides optical (since 1972) and thermal (since 1982) satellite imagery that enables change detection to be monitored. In this study, the change of LULC in 35 years, in five-year periods in the selected area in Buyukcekmece district of Istanbul Megacity was investigated. Rapid urbanization in the region, a green area in 1985, has destroyed especially forest and vegetation areas. Such land cover change is the leading cause of urban heat islands and adversely affects human health and living standards [2, 5]. Besides, land surface temperature (LST) was calculated to show the urban heat intensity's effect using Landsat thermal bands. LST is directly related to the land use and land cover classes and shows low temperature in green spaces, unlike urban areas [5, 6]. This study examined the relationship between the LULC change in the region and the LST change caused by urbanization.

Urban ground subsidence is common phenomenon in cities with dense urbanization, and increased urban expansion triggers land subsidence [7]. The stability of the structures can be affected by various factors like earthquakes [8], construction sites around the buildings [9], and geological conditions of the ground [10] in dense urbanization sites. Synthetic Aperture Radar Interferometry (InSAR) is an ideal solution for observing surface deformation, and it is possible to monitor spatial extension and temporal evaluation of subsidence, especially in the reclamation and rapid urbanization areas. InSAR has been widely used for deformation monitoring of rapid urbanization in the studies [11–13]. Compared with traditional methods such as leveling and global positioning systems (GPS), InSAR has advantages with short revisit times and large-scale monitoring, and these types of passive systems are not affected by weather conditions. Furthermore, it measures surface deformation at millimeter accuracy at both regional and local scales [11]. Especially time series InSAR methods such as Persistent Scatter Interferometry (PSI) and Small

Baseline Subsets (SBAS), which are commonly used, are preferred to detect slow movement. PSI identifies the movement of pointwise targets called "persistent scatterers" like buildings, whereas the SBAS method is more suitable for rural areas [12]. In the study area, the PSI time series InSAR method was selected for observing surface deformation due to its ability to detect urban subsidence, and results were evaluated.

In summary, this study investigated two issues: (i) the effects of rapid urbanization by evaluating temporal change analysis of LULC and LST, (ii) stability of the structures in rapid urbanization sites with time series InSAR analysis. Optical bands of Landsat were used for temporal change analysis, and thermal bands were used for LST analysis. The normalized difference vegetation index (NDVI), the most widely used plant index, was used to determine the temporal change. Sentinel-1 SAR images were used for InSAR analysis. All the obtained results were evaluated together.

2 Related Works

With classification methods and spectral indices, optical remote sensing data has been widely used to detect urban extension. Besides that, many studies have presented urban growth effects on the LULC change using thermal bands. Bhatta et al. (2010) used three Landsat temporal images at 15-year intervals (1975, 1990, and 2005) to determine the urban extent and growth of Kolkata-Howrah [14]. Xiong et al. (2012) investigated the spatiotemporal variations in the LST and LULC types over different urban/rural zones to determine the impacts of rapid urbanization using quantitative thermal remote sensing and spatial statistics methods. The normalized difference built-up index (NDBI) and NDVI were applied to determine the LULC variation in the study, in which Landsat images from four different dates were used. It was seen that while LST was related positively with NDBI and negatively with NDVI [15]. Villa (2012) used Landsat images to determine urban growth in terms of impervious surface expansion of Milan city over 20 years (1984–2003). In the study, soil and vegetation index (SVI), a spectral index aiming to distinguish between urban and non-urban land cover, was applied [16]. Dadras et al. (2015), using aerial photographs and satellite images from 5 different periods between 1956 and 2012, investigated the expansion of the boundaries of the city of Bandar Abbas. In the study, in which they determined the extent of expansion towards 32 different geographical directions, Landsat satellite images were used, and the classification method was applied to the images [17]. Singh et al. (2017) investigated the negative impact of urbanization and its effect on the increasing trends of temperature and degradation of urban ecology by using the Landsat optic and thermal images of Lucknow city, India [18]. Bala et al. (2021) analyzed LST variation with land cover changes in Varanasi city of India from 1989 to 2018 using Landsat satellite images. They applied the random forest classification algorithm for the classification of optical images [19]. Wang et al.

(2021) investigated the spatial distribution and influencing factors on LST in twelve cities of Chine between 2000 and 2017 using temperature and spectral vegetation, built-up, and water indices [20].

In their study, Lei et al. (2018) have aimed to extract all possible information from SAR-InSAR data of Hong Kong city and assess to which extent this information can be exploited for change detection purposes. High-resolution optical images were used for comparison and comprehension. PSI is used to monitor subsidence and uplift phenomena in several cities around the world [21]. Aslan et al. (2018) investigated the spatial extent and rate of ground deformation in the Istanbul megacity by combining InSAR datasets obtained from multiple satellites (291 images in total) and analyzing permanent scatterers. They created maps of the average velocity of ground surface displacement in selected regions [22]. In a study conducted in Italy, the aim was to exemplify a typical subsidence issue related to external loads (urbanization) and a local geological and geotechnical setting (i.e., a subsoil composed of alluvial and coastal compressible deposits). The study evaluates the quantitative contribution of InSAR over a broader perspective of land-use planning and risk management [23]. In their study, Delgado Blasco et al. (2019) conducted urban deformation analysis of the Rome metropolitan area using Sentinel-1 SAR data and the PSI method [24].

3 Materials and Methods

3.1 Study Area

Cities with more than 10 million are called megacities, and Istanbul is one of the 33 megacities in the world with a population of 15.5 million, according to 2020 population data. Its annual growth rate is about twice the general average of Turkey due to internal migration, making it one of the fastest-growing cities in Europe [25]. Due to migration from other cities, urbanization has rapidly increased from the past to the present. According to CORINE land cover inventory, artificial surfaces in Istanbul have increased approximately 72% between 1990 and 2018 [26]. Especially study site (Fig. 1), located in Buyukcekmece district, is under the dense urbanization process.

Buyukcekmece is one of the 39 districts in Istanbul and is a developing district in terms of urbanization and population. In 2020, Buyukcekmece had a 12.7% population growth [27]. Rapid growth leads to rapid urbanization. According to the temperature parameter provided by the Turkish State Meteorological Service, in the last five years temperature of this district has risen by approximately 2 ºC, which is shown in Fig. 2.

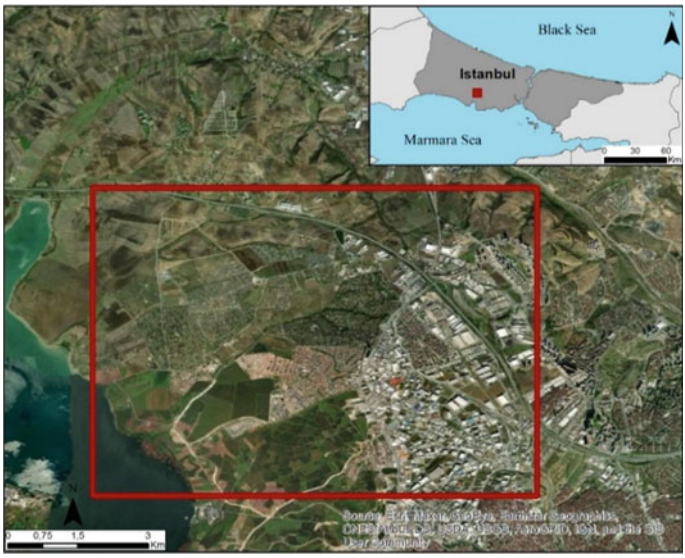

Fig. 1 Study area on Google Earth satellite image

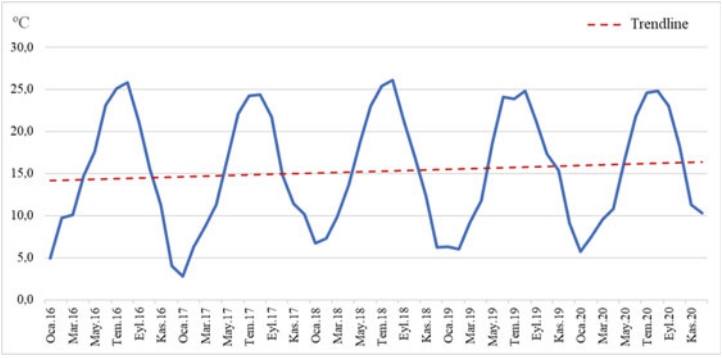

Fig. 2 Monthly Average Temperature of Buyukcekmece Meteorological Station between 2016 and 2020

3.2 Materials

Landsat Level 1 reflectance images which are radiometrically and geometrically corrected, were used to show the urban extension of the study site. Temporal analysis was made with five years period using Landsat 5 TM (Thematic Mapper) and Landsat 8 OLI (Operational Land Imager) satellite images. Optical satellite images are affected by the weather condition, mainly cloudy weather. That is why satellite images were selected in July, considering cloud coverage of scenes except

Table 1 Characteristics of the optical satellite images

Resolution/ Satellite image	Landsat 5 TM	Landsat 8 OLI
Spectral res. (μm)	Blue: 0.45–0.52 Green: 0.52–0.60 Red: 0.63–0.69 Near Infrared: 0.76–0.90 Shortwave Infrared1: 1.55–1.75 Shortwave Infrared2: 2.8–2.35 Thermal: 10.40–12.50	Coastal aerosol: 0.43–0.45 Blue: 0.45–0.51 Green: 0.53–0.59 Red: 0.64–0.67 Near Infrared: 0.85–0.88 Shortwave Infrared1: 1.57–1.65 Shortwave Infrared2: 2.11–2.29 Panchromatic: 0.50–0.68 Cirrus: 1.36–1.38 Thermal1: 10.60–11.19 Thermal2: 11.50–12.51
Spatial res.	Blue, Green, Red, Near Infrared, Shortwave Infrared1-2: 30 m Thermal: 120* (30) m	Panchromatic: 15 m Costal, Blue, Green, Red, Near Infrared, Shortwave Infrared1-2: 30 m Thermal1-2: 100 m
Radiometric res.	8 bits	12 bits
Temporal res. (day)	16	16
Date	July 1, 1985 July 10, 2000 July 31, 1990 July 24, 2005 July 13, 1995 May 3, 2010	July 20, 2015 July 1, 2020

2010. Because of cloudy weather, a satellite image in May was used for 2010. The properties of the Landsat satellite images used are given in Table 1.

The optical satellite images were analyzed using Google Earth Engine cloud-based platform, a free platform that enables geospatial analysis using satellite images [28]. In addition, Sentinel-1 satellite images were used for the time series deformation analysis of the urban area. 145 ascending SLC scenes were processed with only VV polarization. Temporal resolution of Sentinel-1 is 6 days in Europe. Properties of Sentinel-1 are given in Table 2.

Table 2 Properties of SAR images

Satellite	Polarization	Orbit direction	Time period	Number of images	Temporal res.
Sentinel-1 C band	VV	Ascending	November 05, 2018 March 24, 2021	145	6 days

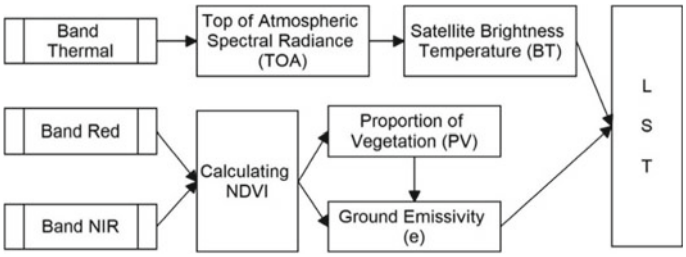

Fig. 3 Flowchart of the Land Surface Temperature (LST) algorithm

3.3 Method

Normalized Difference Vegetation Index (NDVI). NDVI, which is used to detect vegetation cover area on the Earth's surface, is calculated using the near-infrared (NIR) and red bands of the optical satellite images (Eq. 1). NDVI values vary between −1 to +1. Poor vegetation areas like built-up and barren land values are around zero, and healthy vegetation values are close to +1. Water bodies have negative values around −1.

$$NDVI = (NIR - Red)/(NIR + Red) \tag{1}$$

Land Surface Temperature (LST). LST extraction with satellite images is possible using many algorithms [29]. Some of these used algorithms are SplitWindow Algorithm (SWA), Single Channel Algorithm (SCA), Mono-Window Algorithm (MWA), and Radiative Transfer Equation (RTE) [30]. In this study, MWA was used to generate LST maps [31, 32]. The process flow of the methodology is given in Fig. 3.

For this algorithm, firstly, the thermal band formulated from the USGS official site is entered. Then Digital numbers (DN) refer to reflectance values are converted to radiance values. Spectral radiation is converted to brightness temperature (BT) using thermal constants provided in the metadata file of the thermal band data [33]. The Kelvin conversion is performed to get the results in Celsius (about −273.15).

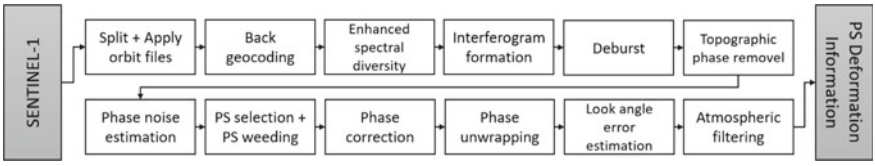

Fig. 4 Flowchart of the PSI method using Sentinel-1

The calculated NDVI was used both in the step of calculating the emission in the LST and in the step of comparing the existing vegetation areas between the LST [34]. The land surface emission (ε) needs to be determined to produce the LST map,. Surface emissivity is defined as the relative ability of the surface of a material to emit energy by radiation. The emissivity is also expressed as the ratio of the energy emitted by a given material to the energy emitted by a black body at the same temperature. In short, it is the efficiency of transmitting thermal energy from the surface to the atmosphere [35]. Equation 2 and Eq. 3 are applied to obtain the land surface temperature map [33]. In the equations, σ is Boltzmann constant (1.38×10^{-23} J/K), h is Planck's constant (6.626×10^{-34} Js), and c is the velocity of light (2.998×108 m/s).

$$\mathrm{LST} = \mathrm{BT} / \{1 + [(\lambda \mathrm{BT}/\rho) \times \ln(\varepsilon)]\} \tag{2}$$

$$\rho = h \times (c/\sigma) = 1.438 \times 10^{-2} \mathrm{m\ K} \tag{3}$$

Persistent Scatter Interferometry (PSI). PSI method was developed twenty years ago for time series deformation analysis of persistent scatters (PS) [36, 37]. This method uses a stack of co-registered SAR images and finds PS points using amplitude and phase variations from the images. Time-series deformation analysis is based on the phase information of the PS points. They are stable artificial objects like buildings and monuments or natural objects and could not be found in rural areas [12]. The steps of the PSI time series InSAR method are given in Fig. 4.

SAR satellite images are split according to the study area before interferometric analysis. Orbital correction is applied using orbit files, and slave images are co-registered to the selected master image. After the interferograms are created for each pair, the topographic phase is removed from the interferograms. According to the calculated phase noise estimation value for each candidate pixel, PS pixels are selected from amplitude dispersion [37]. Amplitude dispersion is taken as between 0.4–0.42, which are reasonable values. After the initial selection step, noisy PS pixels are discarded. The wrapped phase is corrected for spatially uncorrelated look angle error and is unwrapped. Atmospheric filtering is applied using the Delaunay triangulator after look angle error estimation. Obtained deformation results are exported to geographical information systems for the overall assessment of rapid urbanization.

4 Results and Discussion

4.1 Detection of Urban Area Extension

To show changes in the vegetation coverage and extension of urbanization, NDVI was calculated using Landsat 5 TM and Landsat 8 OLI satellite images between

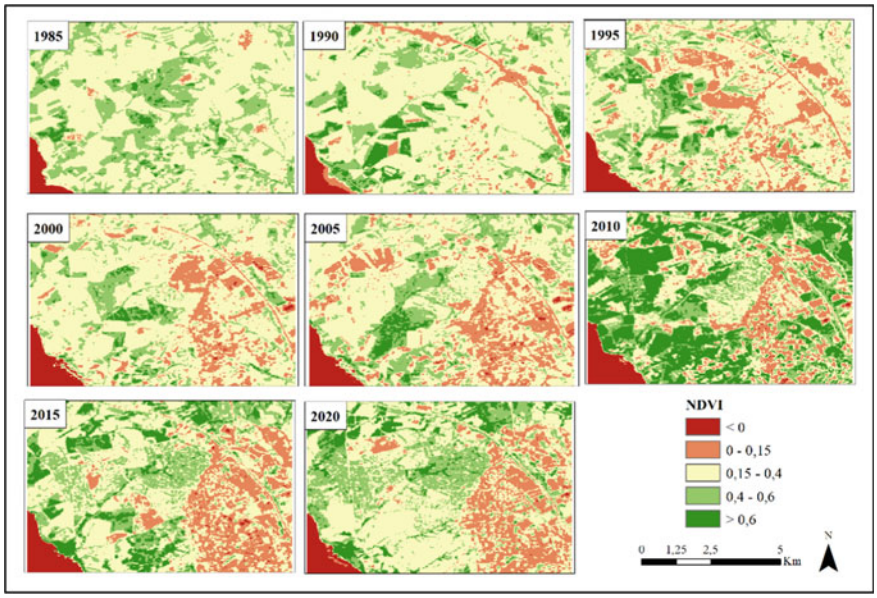

Fig. 5 NDVI density map of study site between 1985–2020 with 5 years period

1985 and 2020 with five years period. With this purpose, NDVI density was determined in five categories as water body (NDVI < 0), built-up (0 < NDVI < 0.15), low vegetation (0.15 < NDVI < 0.4), medium vegetation (0.4 < NDVI < 0.6), and high vegetation (0.6 < NDVI). Produced NDVI density maps for the aforementioned images are shown in Fig. 5. It is clearly observed that the built-up area has covered a large part of the study site.

The areal extension of five NDVI density classes was calculated as a time series analysis in Fig. 6. The built-up area has extended from 57.1 ha to 781.4 ha in the study area. The right part of the urbanization was clearly detected with NDVI

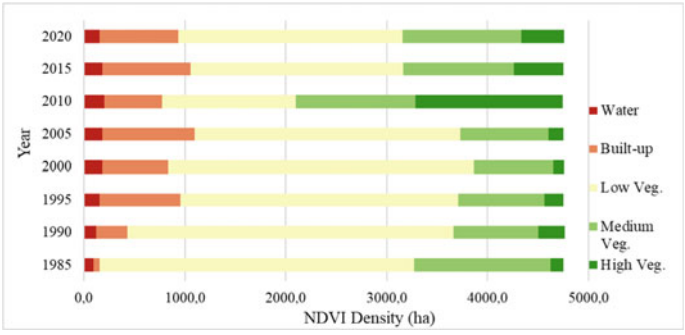

Fig. 6 The areal distribution of NDVI density values between 1985–2020

results; however, the detection of the left part has not been successful because of having green spaces between buildings and the medium spatial resolution of the Landsat (30 m). Therefore, the area of the built-up class is more than detected 781.4 ha.

Whereas the low and medium vegetation area has decreased, high vegetation has increased in this time interval. In 2010, the change in high vegetation class was due to the use of satellite imagery acquired in May having dense vegetation. Additionally, the coastline of the water body has changed, and the surface area of the water has increased from 94.07 ha to 154.8 ha.

4.2 Land Surface Temperature (LST)

LST was applied to selected images, and results are given in Fig. 7. It is clearly observed that the temperature on the urbanization site increased to 45 ºC. The average temperature of 1985 is 26.1 ºC and 2020 31.5 ºC. Average temperature has increased 5.4 ºC because of converting natural LULC to artificial surfaces.

In the study area, there are two types of regions that can be divided as having green spaces or not. These regions are shown with red circles in Fig. 8a for 2020. Urban expansion in Region 2 can be clearly extracted with the NDVI map (Fig. 8b), and LST has reached 45 ºC (Fig. 8c). Unlike Region 2, Region 1 entered the mostly medium vegetation class in the NDVI map (Fig. 8b). The reason for that is to cover empty spaces with green spaces. Additionally, because of the spatial

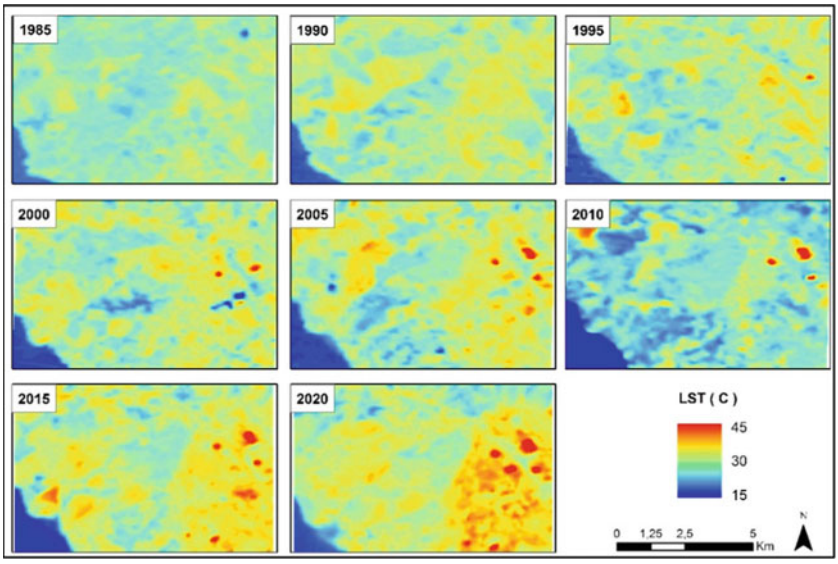

Fig. 7 The Distribution of LST between 1985–2020

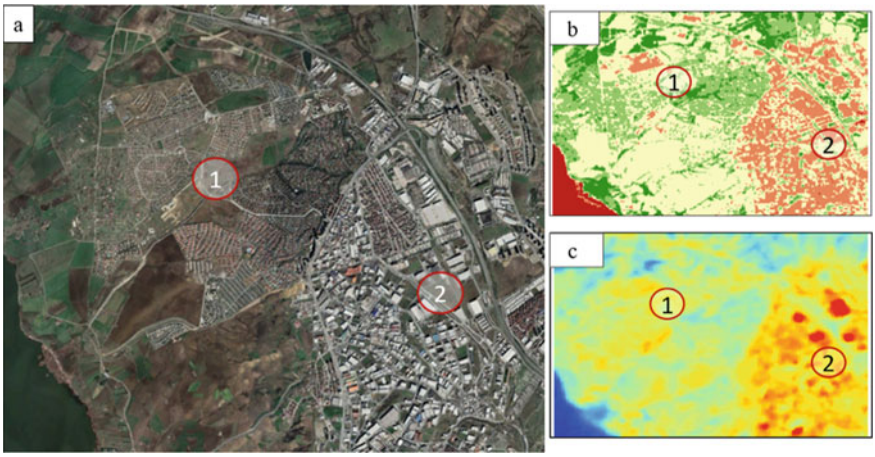

Fig. 8 For 2020, study region's; **a** Google Earth image, **b** NDVI classified map, **c** LST map

resolution (30 m) of Landsat satellite images, these sites were detected as medium vegetation class. Therefore, because of the above-stated reason, LST values of Region 1 have not increased as much as Region 2. This situation also reveals the importance of landscaping.

4.3 Time Series Deformation Analysis

A deformation velocity map of the study site was obtained using the PSI multi-temporal InSAR method. The SLC image acquired on November 30, 2019, was chosen as the master image, and the other 144 images acquired between November 2018 and March 2021 were selected as the slave images. The produced velocity map is shown in Fig. 9a. While blue points show uplift area, red points show the subsidence in line of sight (LOS) direction. A close view of the recent urbanization site is given in Fig. 9b. The time series of PS points showing uplift and subsidence movement in the white circle is given in Fig. 9c with the same color in the velocity map.

The red points in Fig. 9b show that the subsidence of the buildings and construction sites in the middle of buildings can be one of the main reasons for the subsidence. Another reason is the ground stability of the region. Istanbul Metropolitan Municipality (IMM) carried out a landslide awareness project and prepared reports for all districts in Istanbul. In the created report for the Buyukcekmece district, a landslide activity status map was generated considering geological conditions, soil properties, and risk factors [38]. According to generated landslide activity status map, and study area covers passive landslide region which has the potential for a landslide. Additionally, approximately 30% of the landslides

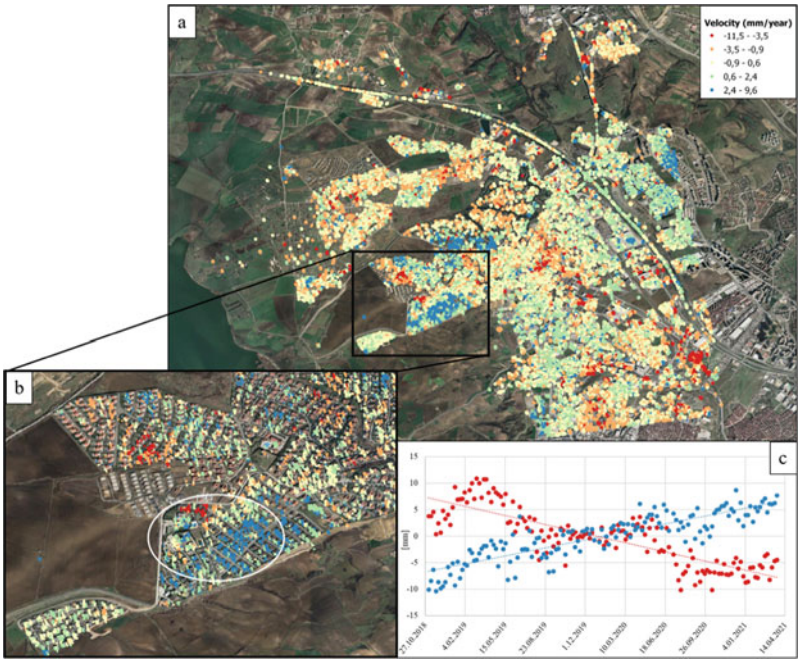

Fig. 9 **a** PSI deformation analysis results over the region, **b** a close view of the new urbanization site, **c** time series of the red and blue points in the white circle

were activated by human impact events. These effects are mainly caused by filling the crown of the landslides, constructing high-rise buildings on the crown of the landslides, and digging the heel of the landslide [39].

Bayik et al. (2021) also evaluated Buyukcekmece – Esenyurt region with the PSI method using ALOS-2 and Sentinel-1 SAR images between 2015–2020 and related with GNSS measurements and landslide inventory map to explain movements characteristics [40]. The region showed as a white circle in Fig. 9b was also evaluated in their study, and subsidence has been detected up to 10 mm in the last 5 years. In this study, however, PS points in the same region were detected as green and yellow color points, which are more stable than the others. It means that as long as the ground settlements are not exposed to other external factors and are not built in areas that will trigger landslides, they become stable over time.

5 Conclusion

Human activities like urbanization can disrupt the Earth's natural balance if it is not controlled. In the study, the urbanization effects were evaluated in two aspects. The first aspect is the urbanization effects on the Earth's surfaces and natural balance;

the second is the effects of the ground movements and construction sites on structural stability in the rapidly urbanized region. Effects on the Earth's surfaces were determined with NDVI indices to determine LULC change and LST to explain urbanization's urban heat island effect. Both of the methods showed successful results. LULC has significantly changed, and LST has increased 5.4 ºC in the study site. Furthermore, according to results, it is obtained that landscaping converting empty spaces with green spaces decreases the effects of the urban heat islands.

In the second aspect, it is observed that construction sites can cause the surrounding buildings to collapse. Additionally, urbanization in the risky sites, sensitive to landslides, comes up against ground movement and deformation. Multi-temporal InSAR is a powerful tool to present the actual condition of the building, and the PSI method showed the deformations caused by construction sites and ground stability. Therefore, it is important to monitor risky sites, and this will prevent disasters that may occur. For more detailed analysis, high-resolution optical and SAR satellite images can be used; but these free satellite images are cost-effective and more useful for a continuous monitoring system.

References

1. N.B. Grimm et al., Global change and the ecology of cities. Science **319**(5864), 756–760 (2008)
2. H. Luo, J. Wu, Effects of urban growth on the land surface temperature: a case study in Taiyuan, China. Environ. Dev. Sustain. **23**, 10787–10813 (2021)
3. L.W. Lai, W.L. Cheng, Air quality influenced by urban heat island coupled with synoptic weather patterns. Sci. Total Environ. **407**(8), 2724–2733 (2009)
4. R. Yao et al., Long-term trends of surface and canopy layer urban heat island intensity in 272 cities in the mainland of China. Sci. Total Environ. **772**, 145607 (2021)
5. B. Halder, J. Bandyopadhyay, P. Banik, Monitoring the effect of urban development on urban heat island based on remote sensing and geo-spatial approach in Kolkata and adjacent areas, India. Sustain. Cities Society **74**, 103186 (2021)
6. R. Amiri, Q. Weng, A. Alimohammadi, S.K. Alavipanah, Spatial–temporal dynamics of land surface temperature in relation to fractional vegetation cover and land use/cover in the Tabriz urban area, Iran. Remote Sens. Environ. **113**(12), 2606–2617 (2009)
7. S. Guo, et al., Deformation velocity monitoring in kunming city using ascending and descending sentinel-1A data with SBAS-InSAR technique, in *IGARSS 2020–2020 IEEE International Geoscience and Remote Sensing Symposium* (IEEE 2020), pp. 1993–1996
8. G.X. Liu, X.L. Ding, Z.L. Li, Z.W. Li, Y.Q. Chen, S.B. Yu, Pre-and co-seismic ground deformations of the 1999 Chi-Chi, Taiwan earthquake, measured with SAR interferometry. Comput. Geosci. **30**(4), 333–343 (2004)
9. N. Yagmur, E. Erten, N. Musaoglu, How to start gentrification process using interferometric stack of SENTINEL-1. ISPRS-Int. Arch. Photogram. Remote Sens. Spat. Inf. Sci. **43**, 183–188 (2021)
10. S. Stramondo, F. Bozzano, F. Marra, U. Wegmuller, F.R. Cinti, M. Moro, M. Saroli, Subsidence induced by urbanisation in the city of Rome detected by advanced InSAR technique and geotechnical investigations. Remote Sens. Environ. **112**(6), 3160–3172 (2008)

11. L. Solari, A. Ciampalini, F. Raspini, S. Bianchini, S. Moretti, PSInSAR analysis in the Pisa urban area (Italy): a case study of subsidence related to stratigraphical factors and urbanization. Remote Sens. **8**(2), 120 (2016)
12. G. Chen, Y. Zhang, R. Zeng, Z. Yang, X. Chen, F. Zhao, X. Meng, Detection of land subsidence associated with land creation and rapid urbanization in the chinese loess plateau using time series insar: a case study of Lanzhou new district. Remote Sens. **10**(2), 270 (2018)
13. S. Jiao, J. Yu, Y. Wang, L. Zhu, Q. Zhou, Estimating the impact of urban expansion on land subsidence using time series of dmsp night-time light satellite imagery. Int. Arch. Photogram. Remote Sens. Spatial Inf. Sci. **42**(3), 691–698 (2018)
14. B. Bhatta, S. Saraswati, D. Bandyopadhyay, Quantifying the degree-of-freedom, degree-of-sprawl, and degree-of-goodness of urban growth from remote sensing data. Appl. Geogr. **30**(1), 96–111 (2010)
15. Y. Xiong, S. Huang, F. Chen, H. Ye, C. Wang, C. Zhu, The impacts of rapid urbanization on the thermal environment: a remote sensing study of Guangzhou, South China. Remote Sens. **4** (7), 2033–2056 (2012)
16. P. Villa, Mapping urban growth using soil and vegetation index and landsat data: the Milan (Italy) city area case study. Landsc. Urban Plan. **107**(3), 245–254 (2012)
17. M. Dadras, H.Z. Shafri, N. Ahmad, B. Pradhan, S. Safarpour, Spatio-temporal analysis of urban growth from remote sensing data in Bandar Abbas city, Iran. Egypt. J. Remote Sens. Space Sci. **18**(1), 35–52 (2015)
18. P. Singh, N. Kikon, P. Verma, Impact of land use change and urbanization on urban heat island in Lucknow city, Central India. A remote sensing based estimate. Sustain. Cities Society **32**, 100–114 (2017)
19. R. Bala, R. Prasad, V.P. Yadav, Quantification of urban heat intensity with land use/land cover changes using Landsat satellite data over urban landscapes. Theoret. Appl. Climatol. **145**, 1–12 (2021)
20. Y. Wang et al., Spatial distribution and influencing factors on urban land surface temperature of twelve megacities in China from 2000 to 2017. Ecol. Indicators **125**, 107533 (2021)
21. L. Lei, D. Perissin, Y. Qin, Change detection with spaceborne InSAR technique in Hong Kong, in *2013 IEEE International Geoscience and Remote Sensing Symposium-IGARSS* (IEEE 2013), pp. 338–341
22. G. Aslan, Z. Cakır, S. Ergintav, C. Lasserre, F. Renard, Analysis of secular ground motions in Istanbul from a long-term InSAR time-series (1992–2017). Remote Sens. **10**(3), 408 (2018)
23. F. Bozzano, C. Esposito, P. Mazzanti, M. Patti, S. Scancella, Imaging multi-age construction settlement behaviour by advanced SAR interferometry. Remote Sens. **10**(7), 1137 (2018)
24. J.M. Delgado Blasco, M. Foumelis, C. Stewart, A. Hooper, Measuring urban subsidence in the Rome metropolitan area (Italy) with Sentinel-1 SNAP-StaMPS persistent scatterer interferometry. Remote Sens. **11**(2), 129 (2019)
25. UN:https://www.un.org/en/events/citiesday/assets/pdf/the_worlds_cities_in_2018_data_booklet.pdf. (2018).
26. CORINE (2020). https://land.copernicus.eu/
27. TUIK (2020). https://www.tuik.gov.tr/
28. N. Gorelick, M. Hancher, M. Dixon, S. Ilyushchenko, D. Thau, R. Moore, Google Earth Engine: planetary-scale geospatial analysis for everyone. Remote Sens. Environ. **202**, 18–27 (2017)
29. B. Yamak, Z. Yagcı, B.B. Bilgilioglu, R. Comert, Investigation of the effect of urbanization on land surface temperature example of Bursa. Int. J. Eng. Geosci. **6**(1), 1–8 (2021)
30. M. IsayaNdossi, U. Avdan, Application of open source coding technologies in the production of land surface temperature (LST) maps from Landsat: aPyQGIS plugin. Remote Sens. **8**(5), 413 (2016)
31. Z. Qin, A. Karnieli, P. Berliner, A mono-window algorithm for retrieving land surface temperature from Landsat TM data and its application to the Israel-Egypt border region. Int. J. Remote Sens. **22**(18), 3719–3746 (2001)

32. F. Wang, Z. Qin, C. Song, L. Tu, A. Karnieli, S. Zhao, An improved mono-window algorithm for land surface temperature retrieval from Landsat 8 thermal infrared sensor data. Remote Sens. **7**(4), 4268–4289 (2015)
33. S.K. Akher, S. Chattopadhyay, Impact of urbanization on land surface temperature-a case study of Kolkata New Town. Int. J. Eng. Sci. **6**(1), 71–81 (2017)
34. U. Avdan, G. Jovanovska, Algorithm for automated mapping of land surface temperature using LANDSAT 8 satellite data. J. Sensors **2016**, 1–8 (2016). https://doi.org/10.1155/2016/1480307
35. J.C. Jimenez-Munoz, J.A. Sobrino, A. Gillespie, D. Sabol, W.T. Gustafson, Improved land surface emissivities over agricultural areas using ASTER NDVI. Remote Sens. Environ. **103** (4), 474–487 (2006)
36. A. Ferretti, C. Prati, F. Rocca, Nonlinear subsidence rate estimation using permanent scatterers in differential SAR interferometry. IEEE Trans. Geosci. Remote Sens. **38**(5), 2202–2212 (2000)
37. A. Ferretti, C. Prati, F. Rocca, Permanent scatterers in SAR interferometry. IEEE Trans. Geosci. Remote Sens. **39**(1), 8–20 (2001)
38. IMM (Istanbul Metropolitan Municipality): Landslide Awareness Booklet of Beylikduzu-Buyukcekmece-Esenyurt Districts (2020). (in turkish)
39. S. Dalgic, M. Turgut, I. Kusku, C. Coskun, T. Cosgun, Impact of soil and rock conditions on building foundations on the european side of Istanbul. Uygulamalı Yerbilimleri Dergisi **8**(2), 47–70 (2009). ((in turkish))
40. C. Bayik, S. Abdikan, A. Ozdemir, M. Arıkan, F.B. Sanli, U. Dogan, Investigation of the landslides in Beylikdüzü-Esenyurt districts of Istanbul from InSAR and GNSS observations. Nat. Haz. **109**, 1–20 (2021)